Synthesis and properties of *in situ* Si_3N_4-reinforced $BaO \cdot Al_2O_3 \cdot 2SiO_2$ ceramic matrix composites

S. W. QUANDER†, A. BANDYOPADHYAY*, P. B. ASWATH‡
Mechanical and Aerospace Engineering Department and Materials Science and Engineering Program, P.O. Box 19031, University of Texas at Arlington, Arlington, TX 76019, USA

Silicon nitride (94.5% α, 5.5% β), $BaCO_3$, Al_2O_3, and SiO_2 powders were mixed and pressureless sintered to produce a ceramic matrix composite consisting of 30 vol% barium aluminosilicate ($BaO \cdot Al_2O_3 \cdot 2SiO_2$ or BAS) matrix reinforced with *in situ* grown whiskers of β-Si_3N_4. *In situ* X-ray studies of the reactions indicated that $BaCO_3$ decomposes first to yield BaO which reacts with SiO_2 to yield a series of barium silicates which then react with Al_2O_3 between 950 and 1300 °C to yield hexacelsian BAS. The sintering times were varied in order to develop a material system that combines the favourable properties of BAS with the high strength of Si_3N_4. *In situ* high-temperature X-ray studies after composite processing did not reveal any changes in the BAS or Si_3N_4 up to temperatures of 1300 °C. Dilatometry studies of the sintered composite indicated a low-temperature transformation between 230 and 260 °C with the temperature of transformation and volume change associated with the hexagonal to orthorhombic transformation decreasing with an increase of sintering time. Room- and high-temperature (1400 °C) strengths were evaluated using four-point bend flexural tests. Composites exhibited near theoretical densities and an increase in flexural strength that was primarily dependent on the higher α- to β-Si_3N_4 transformation.

1. Introduction

Advanced glass-ceramics, such as barium aluminosilicate ($BaO \cdot Al_2O_3 \cdot 2SiO_2$ or BAS) typically exhibit materials properties such as high melting points, low coefficient of thermal expansion, and good dielectric properties [1]. For these reasons, advanced glass-ceramics are worthy of consideration as matrices for ceramic matrix composites with applications in electronic packaging, structural components and nuclear shielding [2–6]. However, like other glass ceramics, the mechanical properties of this material are poor with a reported fracture strength of 80 MPa and fracture toughness of 1.8 $MPa\,m^{1/2}$ [7]. BAS may be strengthened by the addition of silicon nitride (Si_3N_4), which has a covalent bond structure. Properties of Si_3N_4 are reviewed in detail elsewhere [8]. *In situ* growth of β-Si_3N_4 whiskers within BAS, effectively raises the fracture strength of the composite above that of BAS alone. The combination of these two constituents results in composites which combines the favourable physical and electrical properties of BAS with the high strength of Si_3N_4 [9, 10].

BAS exists primarily in three different polymorphs, the monoclinic, hexagonal and orthorhombic phases. The monoclinic phase occurs in nature and is commonly known as celsian, where as the hexagonal phase, which is also known as hexacelsian, and the orthorhombic phases are only found in synthetically produced products [11, 12]. Pure stoichiometric BAS melts at 1760 °C [11]. Below the melting point, the hexagonal hexacelsian phase is thermodynamically stable between 1760 and 1590 °C. Below 1590 °C, celsian or the monoclinic phase is the thermodynamically stable phase [11]. The hexagonal to monoclinic transformation is known to be very sluggish and as a result, the metastable hexagonal phase exists below 1590 °C [13]. At 300 °C, the metastable hexagonal phase transforms to a body centred orthorhombic phase [12, 14]. This is a reversible transformation that is associated with a volume change.

Pressureless sintering offers a low-cost, near-net-shape processing method to produce BAS–Si_3N_4 composites. However, before these materials are used, an extensive analysis of the role of processing variables on the physical and mechanical properties has to be established. The intent of this work was systematically to evaluate the role of sintering time on the porosity content, α- to β-Si_3N_4 transformation,

‡ Author to whom all correspondence should be addressed.
* *Present Address*: Center for Ceramic Research, Rutgers University, P.O. Box 909, Piscataway, NJ 08855, USA.

0022–2461

and mechanical properties of a BAS–Si_3N_4 composite.

2. Experimental procedure

BAS-forming powders consisting of $BaCO_3$ (Mallinchrodt AR Grade), SiO_2 (Nyacol 2034DI) and Al_2O_3 (Baikowski) were mixed with Si_3N_4 (Hermann Starch LC-12S) powders consisting of 94.5% α-Si_3N_4 and 5.5% β-Si_3N_4, along with polymeric binders, in the appropriate ratios to form composites with 70 vol % Si_3N_4 and 30 vol % BAS upon sintering. X-ray diffraction was used to confirm the Si_3N_4 phases present in the starting powders. Constituent materials were wet blended, and milled in ethanol using a high-density polyethylene jar to produce a slurry. The slurry was dried and isostatically pressed at 137 MPa into tests billets which were packed in boron nitride-lined graphite retorts using a powder bed of Si_3N_4-based materials. Sintering was performed in 1 atm nitrogen using heating and cooling rates of 5 °C min^{-1}. Upon sintering, a ceramic matrix composite consisting of Si_3N_4 and BAS was formed. Four billets were fabricated with varying sintering times at a constant sintering temperature of 1800 °C as indicated in Table I.

Bulk densities of all the billets were measured as per ASTM C20-87 [15]. Room-temperature powder X-ray diffraction (XRD) was used to determine the amount of the α- and β-Si_3N_4 present in each of the composite billets. Small samples were cut from the billet, ground and sieved through a -300 mesh screen in preparation for powder XRD. A Phillips PW-1729 diffractometer, utilizing a crystal monochromator using CuK_α radiation and 45 kV and 35 mA power supply, was used with a step size of 0.02° (2θ) and a scan speed of 0.5 s/step. The α- and β-Si_3N_4 contents were calculated using the X-ray diffraction peak height integration method outlined by Gazzara and Messier [16].

High-temperature X-ray diffraction (HTXRD) studies were carried out on powders of particle size of -300 mesh, as well as with solid samples. The temperature was varied incrementally from room temperature to 1400 °C in a SCINTAG, fully automated diffraction system with a copper target operated at 45 kV and 40 mA in an environment of flowing helium. The temperature was held constant to within $\pm$ 1 °C of the set point by using a molybdenum strip heater and a platinum environmental heater, while a scan from 10°–50° (2θ) was made using a step size of 0.02°(2θ) and a count time of 1°(2θ) per minute.

TABLE I Processing variables used to make the Si_3N_4–BAS composites

Composition (vol %)	Sintering temp. (°C)	Sintering time (min)
70% Si_3N_4–30%BAS	1800 °C	1
		30
		120
		180

Dilatometry studies were conducted using a THETA dual push-rod differential dilatometer in the temperature range of 20–1000 °C at a heating and cooling rate of 3 °C min^{-1} in an environment of 1 atm flowing helium. A sample size of 25 mm × 3 mm × 4 mm was used and compared with a sapphire rod as the reference standard. Differential scanning calorimetry was also performed using a Stanton-Redcroft differential scanning calorimeter system employing a heating rate of 10 °C min^{-1} from 20–1450 °C in an environment of flowing argon. Transmission electron microscopy of ion-milled sections of the composites were performed using a Jeol 1200EX.

Four-point bend flexure specimens were machined according to specimen size B of MIL-STD-1942A for each billet fabricated [17]. Specimens measured 3.00 $\pm$ 0.03 mm × 4.00 $\pm$ 0.03 mm × 45 mm (minimum). A test fixture made with high-strength α-SiC with a support span of 40 mm and a load span of 20 mm was used. A crosshead speed of 0.55 mm min^{-1} was employed during testing. Tests were conducted at room temperature and at 1400 °C. Three tests were conducted for each of the sintering conditions. Hydrofluoric acid was used lightly to etch the composites and reveal the morphology of the Si_3N_4 reinforcement. A CRC-100 sputtering unit was used to coat the specimens with a conductive surface of Au–Pd or chromium in preparation for scanning electron microscope (SEM) examinations. Scanning electron microscopy was conducted using a Cambridge 120 Stereoscan SEM.

3. Results

3.1. Processing of BAS–Si_3N_4 composites

BAS-forming powders (i.e. $BaCO_3$, Al_2O_3, and SiO_2) melt during pressureless sintering to form liquid BAS. Within the liquid BAS, equiaxed α-Si_3N_4 transforms to whisker-like β-Si_3N_4 via a three-stage rearrangement/solution–diffusion/precipitation type process [18]. During this transformation, α-Si_3N_4 goes into solution yielding a matrix of BAS supersaturated in silicon and nitrogen. After a short-range diffusion of silicon and nitrogen, nucleation of stable β-Si_3N_4 occurs. In stoichiometric form, the BAS melts at 1760 °C. Upon cooling, the liquid phase crystallizes to form a ceramic matrix composite consisting of a crystalline hexagonal (hexacelsian) BAS matrix reinforced with whisker-like β-Si_3N_4 grains. The α- to β-Si_3N_4 transformation is reported to be a reconstructive transformation of the secondary coordination [19], thus a liquid phase is needed to enable the transformation to occur.

3.2. *In situ* analysis of the phase transformation in the BAS–Si_3N_4 composite

3.2.1. *Room-temperature X-ray diffraction of the presintered and sintered powders*

A mixture of α-Si_3N_4 (95.5% α-Si_3N_4 + 4.5% β-Si_3N_4) powders in the size range of 0.1–10 μm were

mixed with BAS-forming powders $BaCO_3$, Al_2O_3 and SiO_2 to yield a composite with 70% Si_3N_4–30% BAS composite. Fig. 1 shows a room-temperature X-ray diffraction (RTXRD) scan of the powders before sintering. The scan clearly indicates the presence of $BaCO_3$, Al_2O_3 and α-Si_3N_4. The SiO_2 is amorphous and does not show up on the X-ray scan. Fig. 2a, b are the RTXRD scans of the 70% Si_3N_4–30% BAS composite sintered for 1 min (i.e. after heating up to 1800 °C it was held there at temperature for only 1 min) and 180 min at 1800 °C. The X-ray scans indicate that the BAS is hexacelsian with no evidence of the celsian phase, and as the sintering time increases, the α-Si_3N_4 transforms to predominantly β-Si_3N_4.

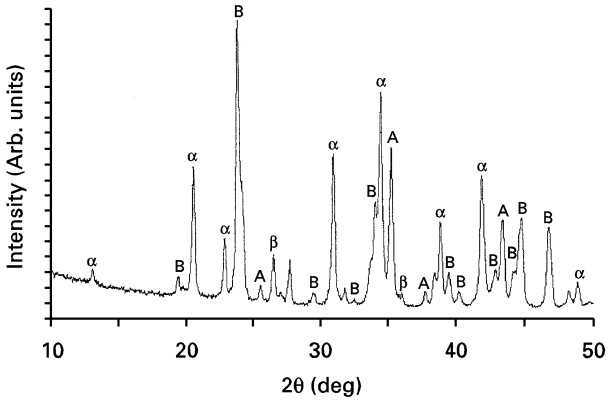

Figure 1 Room-temperature XRD pattern of the presintered powders of $BaCO_3$, (B) Al_2O_3, (A) SiO_2 and Si_3N_4 powders (chosen in a ratio to provide a 70 vol % Si_3N_4–30 vol % BAS when sintered).

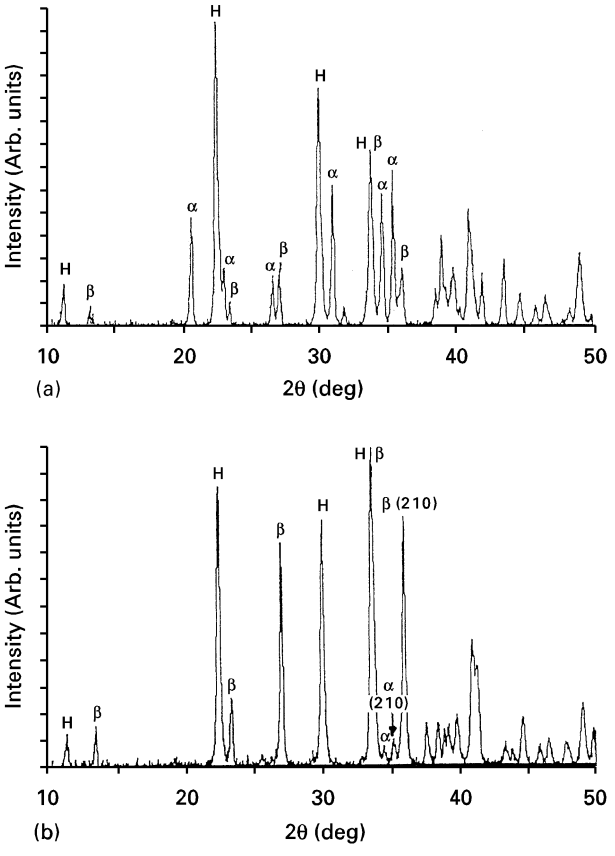

Figure 2 Room-temperature XRD pattern of the 70 vol% Si_3N_4–30 vol% BAS (H = Hexacelsian) sintered for (a) 1 min, and (b) 180 min, at 1800 °C in a nitrogen environment. The plots clearly show an increase in β-Si_3N_4 peaks and a decrease in the α-Si_3N_4 peaks with increase in sintering time. The BAS peaks are unaffected by sintering time.

3.2.2. DSC and high-temperature X-ray diffraction of the presintered powder

Fig. 3 is a DSC scan of the BAS forming powders (i.e. $BaCO_3$, SiO_2, Al_2O_3), α-Si_3N_4 powder mixed together with a polymeric binder. There are endothermic reactions at 640 and 750 °C and exothermic reactions at 820, 1050 and 1200 °C. Based on the DSC results, X-ray scans were performed at room temperature, 500, 690, 950, 1100 and 1300 °C as shown in Fig. 4. The binder burns off at 640 °C, yielding the first endothermic peak. From the high-temperature X-ray diffraction (HTXRD) scans it is apparent that the $BaCO_3$ peaks have diminished at 690 °C with a concurrent increase in the BaO peaks. The second endothermic peak at 750 °C corresponds to the decomposition of $BaCO_3$. At 950 °C there is no BaO present, but evidence of a few barium silicate phases. Owing to the overlapping of the various peaks,

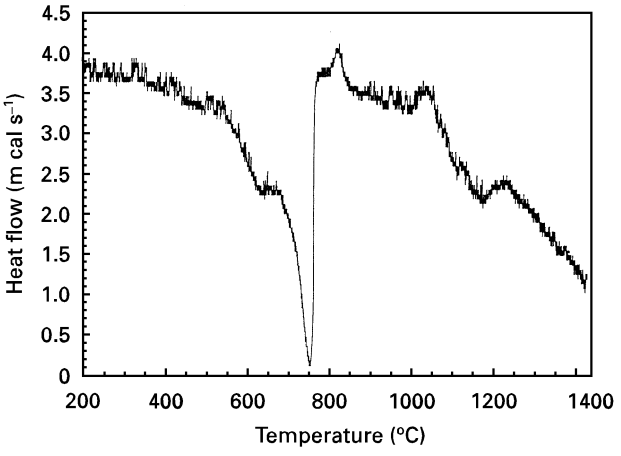

Figure 3 Differential scanning calorimetry scan of the presintered powders heated in an environment of argon at a rate of 10 °C min^{-1}.

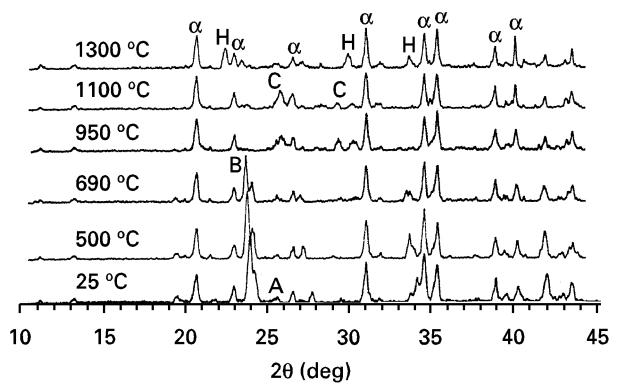

Figure 4 High-temperature powder XRD scan of the presintered $BaCO_3$, (B) Al_2O_3, (A) SiO_2 and Si_3N_4 powders (chosen in a ratio to provide a 70 vol % of Si_3N_4–30 vol % BAS) (H = Hexacelsian) (C = Barium Silicates) at various temperatures in a helium environment.

independent verification of the silicate phases is difficult. However, the dominant silicate peaks are those of $BaO \cdot SiO_2$ and $BaO \cdot 2SiO_2$ and $BaO \cdot 4SiO_2$ to a lesser extent. It can be postulated that the exothermic reactions at 820 °C correspond to the formation of the silicates. The X-ray scan at 1100 °C indicates the presence of small amounts of BAS and some residual barium silicates. At 1300 °C the only phases present are hexacelsian BAS and α-Si_3N_4. At temperatures up to 1300 °C there is no evidence of transformation of the α- to β-Si_3N_4.

3.2.3. High-temperature X-ray diffraction of the postsintered powder

Presented in Fig. 5 are powder XRD patterns of the pressureless sintered 70% Si_3N_4–30% BAS composite sintered for 180 min at 1800 °C in the temperature range of room temperature to 1300 °C. These X-ray scans indicate that the only phases present are hexacelsian BAS and β-Si_3N_4 at all temperatures from room temperature to 1300 °C. No significant changes in the XRD pattern over the temperature range of room temperature to 550 °C indicate that even if there is a hexagonal to orthorhombic transformation in BAS, it is not revealed by XRD. The fact that this transformation is not revealed by XRD agrees quite well with Takéuchi's studies in pure BAS [20].

3.2.4. Low-temperature dilatometry studies

Pure BAS transforms from the hexagonal to orthorhombic form at approximately 300 °C [12]. The hexagonal to orthorhombic transformation is associated with the shifting of the light atom of oxygen [12]. Early high-temperature X-ray studies in pure BAS [20] indicated that no significant differences were observed between the powder diffraction patterns of the hexacelsian and orthorhombic forms of BAS except for a small lattice shift. Structure factor calculations also indicate that XRD is not sensitive to the small shifts of light atoms such as oxygen. Based on these findings, the hexacelsian to orthorhombic transformation was studied using dilatometry, paying particular attention to the role of β-Si_3N_4 on the transformation.

Fig. 6 shows dilatometry scans plotted in terms of linear expansion of the specimen as a function of temperature. These scans plot specimen expansion of the 70% Si_3N_4–30% BAS composite sintered for various times at 1800 °C. The instantaneous coefficient of thermal expansion, which is defined as the differential of specimen expansion with respect to temperature at every temperature, is plotted as a function of temperature in Fig. 7. The width of the peak provides an estimate of the temperature range over which the transformation occurs. Only the heating part of the cycle was plotted in Figs 6 and 7, but a reversible trend was found during cooling as well. The data clearly show that the hexacelsian to orthorhombic transformation is occurring in this temperature range. The linear expansion associated with the hexacelsian to orthorhombic transformation, coefficient of thermal expansion (CTE) and the peak transformation temperature associated with the transformation, are shown in Table II.

It is clear from Fig. 7 that as the extent of β-Si_3N_4 increases, the temperature of the hexacelsian to orthorhombic transformation decreases coupled with a decrease of linear shrinkage. The CTE of the composites is equivalent on either side of the hexagonal to orthorhombic transformation with a sharp change in length at the temperature of transformation, as shown in Fig. 6. The β/α Si_3N_4 ratio does not influence the CTE apart from changing the hexagonal to orthorhombic transformation temperature and linear shrinkage, as shown in Figs 6 and 7, and Table II.

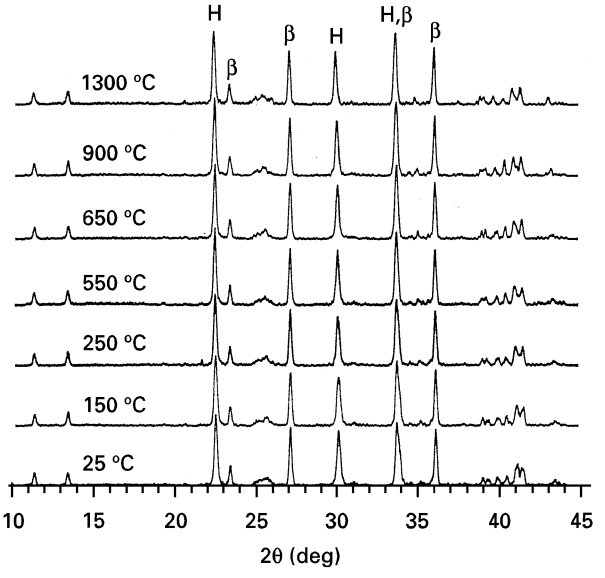

Figure 5 High-temperature powder XRD scan of the 70 vol % of Si_3N_4–30 vol % BAS (H = Hexacelsian) composite sintered for 180 min at 1800 °C at various temperatures in a helium environment.

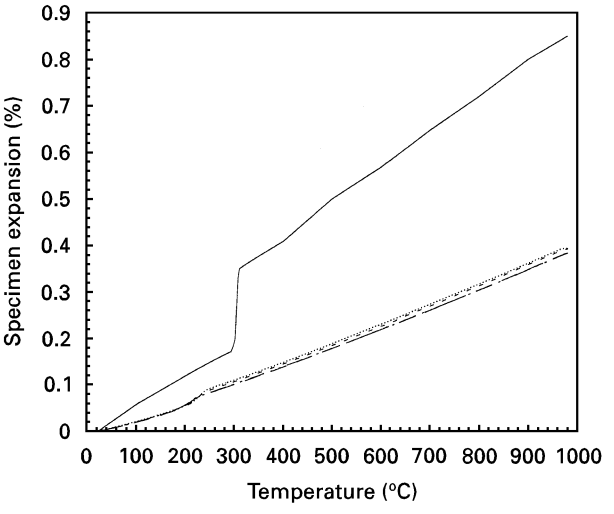

Figure 6 Linear expansion as a function of temperature of the 70 vol % Si_3N_4–30 vol % BAS composite sintered for different periods of time at 1800 °C. Superimposed is the linear expansion of pure hexacelsian BAS as a function temperature [12]. (——) 180 min, (— - —) 120 min, (– – –) 30 min, (···) 1 min, (—) pure BAS.

3.2.5. Extent of densification and the α to β transformation in Si_3N_4

The extent of densification achieved during the liquid-phase sintering process was gauged by examining the per cent theoretical density as a function of sintering time. The extent of the α- to β-Si_3N_4 transformation was determined from XRD data for all sintering times. The β-Si_3N_4 content, Y, was normalized using the formula

$$Y = \left(\frac{\beta}{\alpha + \beta}\right) \times 100 \quad (1)$$

where α is the α-Si_3N_4 content and $\beta = (\beta_0 + \beta_t)$ where β_0 is the initial β-Si_3N_4 content in the powders and β_t is β-Si_3N_4 formed by the α to β transformation in the Si_3N_4. This formula includes the β-Si_3N_4 content in the original forming powders ($\beta_0 = 5.5$ vol %) and that which is formed from the α- to β-Si_3N_4 transformation.

The relationship between the α- to β-Si_3N_4 transformation and densification in the 70% Si_3N_4–30% BAS composites is shown in Fig. 8. The per cent theoretical density, and the extent of the α- to β-Si_3N_4 transformation, are plotted as a function of increasing sintering time. The per cent theoretical density of the 70% Si_3N_4–30% BAS composites was based on a theoretical density of 3.25 g cm^{-3}. Densities as high as 98.5% theoretical were achieved within 1 min sintering. Beyond 1 min there was little increase in theoretical density with sintering time.

The extent of the α- to β-Si_3N_4 transformation increased steadily from 20% after 1 min sintering at 1800 °C, to an excess of 85% after 180 min sintering. Secondary electron SEM images of the composite sintered for 1, 120 and 180 min at 1800 °C are shown in Fig. 9a–c, respectively. Specimens were over-etched to reveal the β-Si_3N_4 distribution. After 1 min sintering, a fine distribution of β-Si_3N_4 whiskers is evident. The largest of these β-Si_3N_4 whiskers measure approximately 1 μm in length and 0.2 μm in width, though there were several more particles which were significantly smaller in the early stages of growth. In addition, globular α-Si_3N_4 which is as yet untransformed, can be seen. After 180 min sintering, a bimodal distribution of β-Si_3N_4 whiskers is apparent. Numerous grains measuring approximately 4–6 μm in length and 1 μm in width are readily apparent, in addition to a large number of grains in the size range 1–2 μm in length and 0.2–0.4 μm in diameter. Bright-field transmission electron micrographs of the composite sintered for 120 and 180 min at 1800 °C are shown in Fig. 10a and b, respectively (the 1 min sintered sample was very brittle and precluded the

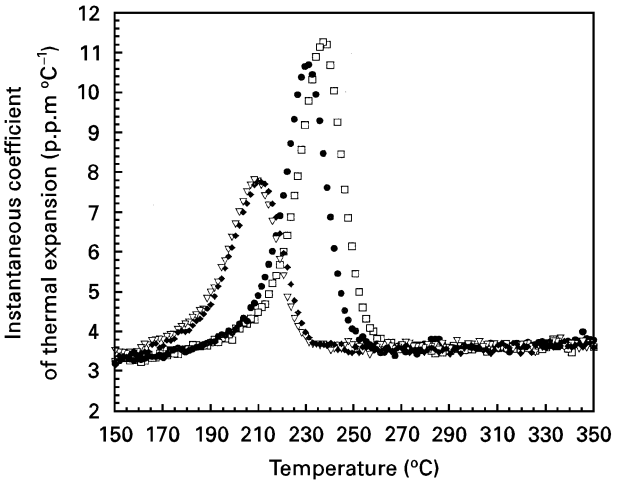

Figure 7 Instantaneous linear coefficient of thermal expansion as a function of temperature of the 70 vol % Si_3N_4–30 vol % BAS composite sintered for different periods of time at 1800 °C: (□) 1 min, (●) 30 min, (▽) 120 min, (◆) 180 min.

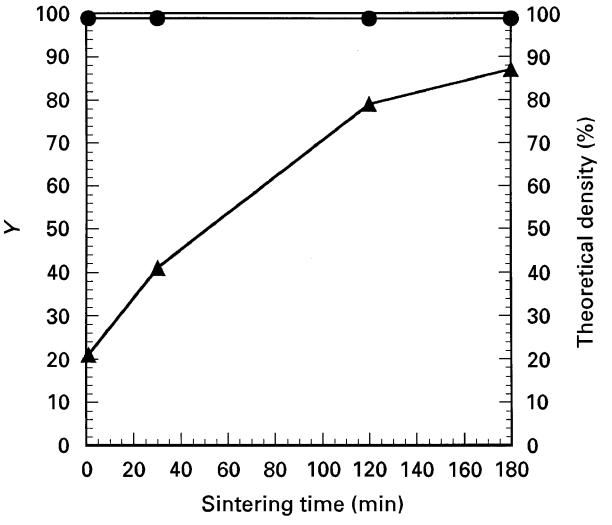

Figure 8 The per cent theoretical density and the extent of α to β transformation in Si_3N_4 as measured by Y, as a function of sintering time in the 70 vol % Si_3N_4–30 vol % BAS composite system. (●) Theoretical density is independent of sintering time, but the amount of β-Si_3N_4 increases with sintering time. (▲) $Y = \beta/(\alpha \times \beta) \times 100$.

TABLE II Coefficient of thermal expansion, peak transformation temperature for the hexagonal to orthorhombic forms of BAS, the transformation temperature range and the percentage of specimen expansion during the transformation

Composition (vol %)	Sintering time (min)	CTE (10^{-6} °C^{-1})	Peak transformation temperature (°C)	Transformation temperature range (°C)	Linear expansion (%)
Pure BAS [5]	–	8.0	300	–	0.15– 0.2
70% Si_3N_4–30%BAS	1	3.5	235	260–175	0.018
70% Si_3N_4–30%BAS	30	3.5	230	255–175	0.017
70% Si_3N_4–30%BAS	120	3.5	210	230–170	0.012
70% Si_3N_4–30%BAS	180	3.5	210	230–170	0.012

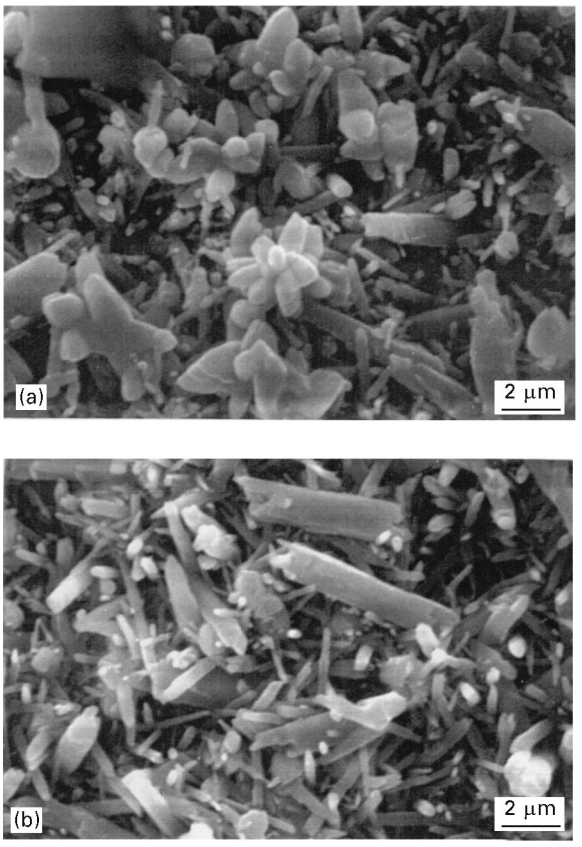

Figure 9 Secondary electron scanning electron micrographs of the etched 70 vol % Si_3N_4–30 vol % BAS composite system sintered for (a) 1 min, and (b) 180 min, at 1800 °C. The micrographs show the increase in the β-Si_3N_4 whisker content with increase in sintering time.

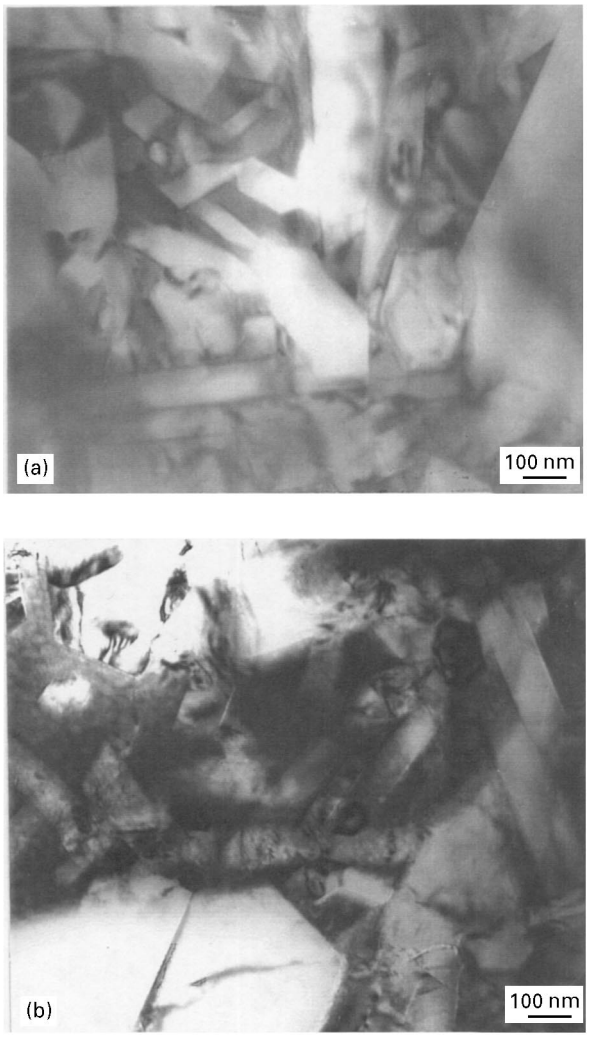

Figure 10 Transmission electron micrographs of 70 vol % Si_3N_4–30 vol % BAS composite system sintered for (a) 120 min, (b) 180 min, at 1800 °C.

preparation of TEM samples). On sintering for 120 and 180 min, well-defined β-Si_3N_4 whiskers are seen. Regions between the whiskers are occupied by BAS. There is no evidence of microcracks at any location in the micrographs. Fig. 2a and b show the powder XRD plots of the 70 Si_3N_4: 30 BAS composite sintered for 1 and 180 min at 1800 °C, respectively. It is clear that there is little change in the BAS peaks on sintering, but the Si_3N_4 peaks exhibit significant changes with the intensity of the α-Si_3N_4 peaks decreasing and the intensity of the β-Si_3N_4 increasing.

3.3. Mechanical properties of the 70% Si_3N_4–30% BAS composite

The influence of increasing sintering time on flexural strength of the 70% Si_3N_4–30% BAS composite is clearly evident in Fig. 11. Room-temperature flexural test results indicate increases in strength from 275 MPa after 1 min sintering of 375 MPa after 180 min sintering. These results represent a significant increase in strength above that of BAS alone, which is reported to have strengths near 80 MPa [7]. Room-temperature load–deflection curves exhibited linear behaviour up to fracture. Comparison of Figs 8 and 10 indicates that the increase in strength at room temperatures arises due to the increased fraction of β-Si_3N_4 which is the only variable that is changing. Fractographs of the flexure failure at room temperature of the composite sintered for 1 and 180 min at 1800 °C, are presented in Fig. 12a and b. The hexagonal cross-section of the β-Si_3N_4 reinforcement is clearly evident in the fractograph from whiskers

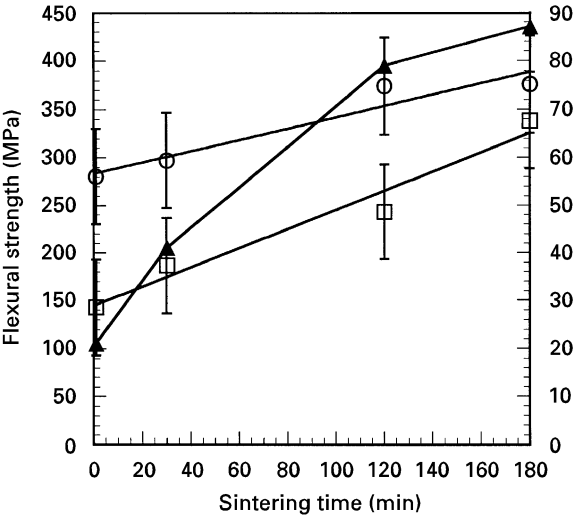

Figure 11 Flexural strength as a function of sintering time in the 70 vol% Si_3N_4–30 vol % BAS composite system at (○) room temperature and (□) 1400°C. Superimposed are the normalized β-Si_3N_4 content as a function of sintering time: (▲) $Y = \beta/(\alpha + \beta) \times 100$.

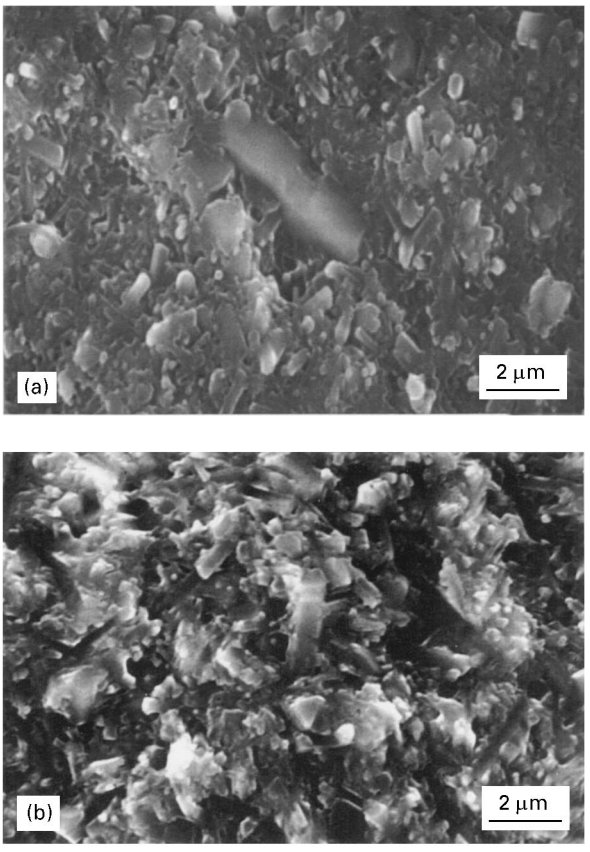

Figure 12 Fracture surface of the 70 Si_3N_4–30 BAS composite sintered for (a) 1 min, and (b) 180 min, at 1800 °C followed by flexure testing at room temperature. The fracture surface exhibits a larger number of β-Si_3N_4 whiskers with increased sintering time which is responsible for the improvement in strength.

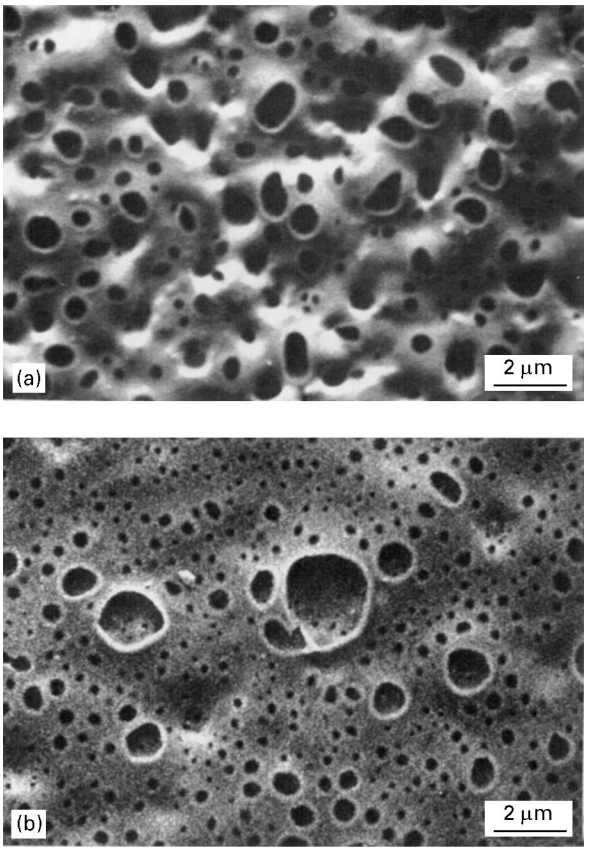

Figure 13 Fracture surface of the 70 Si_3N_4–30 BAS composite sintered for (a) 1 min, and (b) 180 min, at 1800 °C followed by flexure testing at 1400 °C. Melting of the BAS matrix has occurred, possibly due to the presence of some low melting glassy phase.

oriented perpendicular to the fracture plane. The higher aspect ratio of the β-Si_3N_4 whiskers is responsible for the increase in flexure strength with sintering time. High-temperature (at 1400 °C) strengths were found to be 60%–80% of those reported at room temperature, with strengths measuring from 150 MPa after 1 min sintering and 320 MPa after 180 min sintering. High-temperature tests exhibited a non-linear load–deflection curve, suggesting softening of the BAS matrix. This resulted in the flexural strength decreases at elevated temperatures. The strength retention increased with increasing sintering time suggesting the improved reinforcing capability of the β-Si_3N_4 whiskers as compared to the α-Si_3N_4 particles. Fig. 13a and b show fracture surfaces of the composite sintered for 1 and 180 min at 1800 °C, followed by flexure testing at 1400 °C in air. The surface of the high-temperature fracture surface specimen exhibited a white residue/froth which appears as voids, indicating the existence of low-melting glassy phases and/or non-stoichiometric phases. The voids are associated with melting of the matrix preferentially around particles or whiskers. In the specimen sintered for 180 min it appears that there is coalescence of many small voids to form macropores of dimensions as large as 15 μm diameter. The froth formed at the surface of the flexure specimens was scraped and powdered and subjected to powder XRD. The X-ray data only showed the presence of hexagonal BAS peaks without any Si_3N_4 peaks, with no evidence of any new phases. This does not preclude the presence of amorphous phases, as XRD is not a good tool to detect them. Pickup and Brook [21] used components of the $BaO–Al_2O_3–2SiO_2$ system as sintering aids for hot-pressed Si_3N_4. Sintering aids typically range from 5–10 vol % for these types of applications. Their flexure test results [21] indicate a linear elastic behaviour up to failure at both room temperature and 1400 °C. A room-temperature flexure strength of approximately 530 MPa and 1400 °C flexure strength of approximately 320 MPa were reported. They also reported the formation of a high SiO_2 content low-melting non-stoichiometric BAS phase during high-temperature testing. The higher Si_3N_4 content in their composites accounts for the improved room-temperature flexure properties, while the presence of the glassy phase results in similar high-temperature flexure strength. In addition, at 1400 °C, the Si_3N_4 is itself unstable in an air environment and can undergo oxidation to SiO_2. This SiO_2 can react with surrounding BAS and form low-melting amorphous phases.

4. Discussion

The mechanical properties of the BAS–Si_3N_4 composites are accounted for by a synergistic interaction of several factors which include porosity content, total Si_3N_4 content and β-Si_3N_4 content. In recent years,

several researches have also documented the role played by these factors on mechanical properties of composites with large amounts of Si_3N_4 with small additions of oxides as sintering aids [8, 22–24]. Key issues related to the usage of different sources of Si_3N_4 powder properties and their influence on the sintered product have been presented by other researchers [22]. In this study, each material composition was derived from a single source of starting powders.

4.1. Phase transformations in the Si_3N_4–BAS system

DSC scans and *in situ* X-ray studies provide important insight into the phase transformation involved during the processing of the 70% Si_3N_4–30% BAS composites. It is clear that during processing, the first steps involve the elimination of volatiles like the polymeric binders and CO_2 from $BaCO_3$. This is followed by the formation of a series of barium silicates. Al_2O_3 is involved in the reaction only at temperatures greater than 1100 °C to yield hexacelsian BAS. The only form of BAS formed is the hexacelsian form with no evidence of the monoclinic form. The transformation of α- to β-Si_3N_4 only occurs at temperatures greater than 1600 °C, and hence 1800 °C was chosen as the sintering temperature.

Monoclinic celsian is the structure of choice in Si_3N_4–BAS composites because it is the stable phase and does not undergo any transformations at low temperature. In the presence of Si_3N_4 in the matrix, metastable hexacelsian is found to exist to lower temperature, and monoclinic celsian is not evident. In addition, the presence of Si_3N_4 also stabilizes the hexacelsian phase relative to the orthorhombic phase and decreases the linear contraction (and hence the volume change) associated with the hexacelsian to orthorhombic transformation. The extent of this contraction also decreases with tan increase in sintering time which is associated with increased amounts of α to β transformation in the Si_3N_4. The coefficient of thermal expansion of the pure hexagonal BAS structure is $8.0 \times 10^{-6}\,°C^{-1}$ and that of Si_3N_4 is between 2.9×10^{-6} and $3.6 \times 10^{-6}\,°C^{-1}$. As the composite is cooled from the processing temperature, the difference in CTE may lead to residual tensile stresses in the BAS matrix and compressive stresses in the Si_3N_4. The higher aspect ratio of the β-Si_3N_4 may lead to localized residual stresses near the tips of the whisker, while the equiaxed α-Si_3N_4 would have a more uniform residual stress field surrounding it. It is postulated that the presence of the residual tensile stress in the BAS matrix retards the hexagonal to orthorhombic transformation which requires a slight rearrangement of the oxygen atoms.

4.2. Microstructure development

Results indicate that densification and the α to β transformation in Si_3N_4 proceed independently of each other. Composites exhibit rapid sintering at 1800 °C, yielding a dense composite with a bulk density of 98.5% after 1 min sintering. With continued sintering, the β-Si_3N_4 content increases. At 1800 °C, the kinetics of the α to β transformation in Si_3N_4 is very rapid due to the lower viscosity of the BAS matrix which facilitates rapid diffusion. The α to β transformation in Si_3N_4 is a solution–diffusion–precipitation process. This involves the dissolution of the α-Si_3N_4, followed by short-range diffusion of silicon and nitrogen, and eventual reprecipitation of the β-Si_3N_4. The rate of nucleation of β-Si_3N_4 depends on the supersaturation of silicon and nitrogen in the BAS and the kinetics of the transformation depends on the viscosity of the BAS matrix. The 70 Si_3N_4–30 BAS composite has a high supersaturation of silicon and nitrogen by virtue of the higher Si_3N_4 content and a high diffusion rate of silicon and nitrogen due to sintering at 1800 °C. The α to β transformation is very rapid, with as much as 85% of the total Si_3N_4 being β-Si_3N_4 after 180 min sintering.

4.3. Role of total β-Si_3N_4 content in the composites on mechanical properties

It is clear that the β-Si_3N_4 is more efficient as a reinforcement than α-Si_3N_4. This is related to the morphology and distribution of the Si_3N_4. The α-Si_3N_4 is equiaxed and distributed randomly in the BAS matrix and does not serve as an effective reinforcement due to limited load transfer between the particles and the matrix. On the other hand, β-Si_3N_4 has a whisker-like morphology which is more effective as a reinforcement because it enhances the load transfer between the matrix and the whiskers. This is in agreement with the work of other researchers who have examined the role of the aspect ratio of β-Si_3N_4 on the strength of the Si_3N_4 composites with less than 5% oxide content as sintering aid [8, 22–24].

4.4. Role of BAS on the high-temperature strength

BAS, the only ternary compound in the BaO–Al_2O_3–SiO_2 system, was chosen as the matrix material based on the premise that it remains crystalline up to its melting point of 1760 °C. Studies [11] in stoichiometric unreinforced BAS have indicated that a crystalline monoclinic celsian phase is stable upto 1590 °C, at which point it transforms to a hexagonal hexacelsian phase which remains stable to 1760 °C. A cursory look at the quasi-ternary phase diagram [4], for the BaO–Al_2O_3–SiO_2 system, indicates that the presence of excess silica can potentially yield low-melting barium silicates. In the powder XRD studies performed, the matrix does not contain any crystalline phase other than BAS; however, the presence of amorphous barium silicates cannot be independently verified. In their work on hot-pressed 75% Si_3N_4–25% BAS (celsian), Pickup and Brook [21], indicate that 1400 °C strength is limited by the softening of the BAS matrix. In addition, Drummond and Bansal [4] have also indicated that softening of the BAS occurs at temperatures greater than 1000 °C. Similar findings have been reported for hot-pressed and hot isostatically pressed Si_3N_4 composites which

have been limited by softening of residual glassy phases at grain boundaries and triple nodal points [24].

In this study, it is clearly seen in the 70% Si_3N_4–30% BAS composites, that the decrease in the flexure properties at 1400 °C relative to room-temperature properties is maximum at low sintering times, when little of the α to β transformation in Si_3N_4 is complete. It is possible that the excess silicon in the matrix at the early stages of sintering may be responsible for the poor properties. In the composite sintered for 180 min, the flexure strength is approximately 320 MPa at 1400 °C which is similar to the results of Pickup and Brook [21] for the 75% Si_3N_4–25% BAS (celsian) composite. This indicates that the high-temperature properties are primarily controlled by softening of the BAS phase, while the room-temperature properties are controlled by the total Si_3N_4 content and β-Si_3N_4 content.

5. Conclusions

1. Synthesis of Si_3N_4–BAS composites involves the decomposition of $BaCO_3$ followed by the formation of various barium silicates and finally BAS.

2. Densification and α- to β-Si_3N_4 transformation are essentially two independent processes occurring concurrently during sintering.

3. The presence of Si_3N_4 stabilizes the hexagonal hexacelsian phase which later transforms to an orthorhombic phase at lower temperatures. The volume change and temperature of transformation from hexacelsian to orthorhombic phase decrease with an increase in sintering time and is attributed to an increase in the β-Si_3N_4 content in the composite.

4. The 70 Si_3N_4–30 BAS composite developed near theoretical densities after 1 min sintering and showed considerable strength increases with increasing sintering times, which is primarily attributed to an increase in the β-Si_3N_4 content.

5. Flexural tests at 1400 °C exhibited non-linear deformation. There was a significant drop in flexure strength coupled with the presence of frothing on the surface, indicative of an amorphous barium silicate in the matrix.

Acknowledgement

This work was supported in part by NASA as part of the NASA/UTA Center for Hypersonic Research. In addition, support was also provided by the National Science Foundation as part of a Research Initiation Grant no. MSS-9108891. Experimental assistance provided by Mr W. D. Porter and Mr O. B. Cavin, High Temperature Materials Laboratory at Oak Ridge National Laboratory, is gratefully acknowledged. Material processing and coupon machining were performed by Loral Vought Systems and is gratefully acknowledged. The authors thank Dr David. L. Hunn and Mr Douglas Freitag for useful discussions.

References

1. D. BAHAT, *J. Mater. Sci.* **4** (1969) 855.
2. N. P. BANSAL and M. J. HYATT, *ibid.* **24** (1989) 1257.
3. C. H. DRUMMOND III, W. E. LEE, N. P. BANSAL and M. J. HYATT, *Ceram. Eng Sci. Proc.* **9** (1989) 1485.
4. C. H. DRUMMOND III and N. P. BANSAL, *ibid.* **11** (1990) 1072.
5. N. P. BANSAL, M. J. HYATT and C. H. DRUMMOND III, *ibid.* **12** (1991) 1222.
6. C. H. DRUMMOND III, *J. Non-Cryst. Solids* **123** (1990) 114.
7. I. G. TALMY and D. A. HAUGHT, "Ceramics in the System $BaO \cdot Al_2O_3 \cdot SiO_2$–$BaO \cdot Al_2O_3 \cdot 2SiO_2$ for Advanced Radome Application", **NSWC TR 89-162**, Naval Surface Warfare Center (1989).
8. G. ZIEGLER, J. HEINRICH and G. WOTTING, *J. Mater. Sci.* **22** (1987) 3041.
9. K. K. RICHARDSON, D. W. FREITAG and D. L. HUNN, *J. Amer. Ceram. Soc.* **72** (1995) 2662.
10. A. BANDYOPADHYAY, S. W. QUANDER, P. B. ASWATH, D. W. FREITAG, K. K. RICHARDSON and D. L. HUNN, *Scripta Metall. Mater.*, **32** (1995) 1417.
11. H. C. LIN and W. R. FOSTER, *Am. Mineral.* **53** (1968) 134.
12. B. YOSHIKI and K. MATSUMOTO, *J. Am. Ceram. Soc.* **34** (1951) 280.
13. D. BAHAT, *J. Mater. Sci.* **4** (1969) 855.
14. A. BANDYOPADHYAY, P. B. ASWATH, W. D. PORTER and O. B. CAVIN, *J. Mater. Res.* **10** (1995) 1256.
15. ASTM-C20–87, "Standard Test Methods for Apparent Porosity, Water Absorption, Apparent Specific Gravity and Bulk Density of Burned Refractory Brick and Shapes by Boiling Water", Refractories; Carbon and Graphite Products; Activated Carbon; 15.01(5-7) (American Society for Testing and Materials, Philadelphia PA, 1993).
16. C. P. GAZZARA and D. R. MESSIER, *Ceram. Bull.* **56** (1977) 777.
17. MIL-STD-1942A, Department of the Army, Washington DC 20310 (June 1990).
18. S. HAMPSHIRE, "The Sintering of Nitrogen Ceramics", Research Reports in Materials Science Series ed.: P. E. Evans (The Parthenon Press, Lancashire, England, 1986) p. 7.
19. M. J. BUERGER, in "Phase Transformation in Solids" edited by R. Smoluchowski, J. E. Mayer and W. A. Weyl (Chapman and Hall, London, 1951) p. 183.
20. Y. TAKÉUCHI, *Mineral. J.* **2** (1958) 311.
21. H. PICKUP and R. J. BROOK, *Br. Ceram. Soc. Proc.* **39** (1987) 69.
22. G. WOETTING, H. FEUER and E. GUGEL, *Mater. Res. Soc. Proc. Silicon Nitride Ceram.* **287** (1993) 133.
23. G. WOETTING and G. ZIEGLER, *Sci. Ceram.* **12** (1983) 361.
24. G. HIMSOLT, H. KNOCH, H. HUEBNER and F. W. KLEINLEIN, *J. Am. Ceram. Soc.* **62** (1979) 29.

Received 16 February
and accepted 17 September 1996